CYLINDRICAL SHELL ROOFS MADE OF CORRUGATED METAL SHEETS

M. N. EL-ATROUZY
Ain Shams University
Cario, Egypt

This study is presented to establish methods of structural analysis and practical applications of cylindrical shell roofs made of corrugated metal sheets.

The present approach is based on treating the corrugated sheets as orthotropic material and deals with their application in shell roofs.

The exact differential equations governing the behavior of orthotropic shells, derived earlier by the author, are used and solved for different cases of practical boundary conditions. An experimental program was undertaken with full-scale tests on shell roofs. The experimental results showed good agreement with those obtained theoretically.

Simplified formulas were suggested, and design tables were prepared to demonstrate the use of these simplified formulas. One example is included to show the design procedure.

KEYWORDS

Corrugated sheets, orthotropic, roofs, shells.

INTRODUCTION

The use of light-gauge corrugated metal sheets goes back to the beginning of this century. For a long time, corrugated sheets were used as covering materials, without any attention paid to their structural capability. The reason for not considering them as structural elements was the lack of a sound basis for connecting these sheets together to form a continuous medium. Many investigators studied the effect of connecting the sheets together and laid a sound basis for considering the connected sheets as a continuous medium. Nilson was the first to study the behavior of these sheets when assembled.[1] His study laid the foundation for the use of corrugated sheets as shear diaphragms to replace horizontal bracings in steel buildings. Nilson also showed the possibility of using these sheets in folded plate roofs.[2]

Parallel to these studies, extensive study of the structural behavior of such an assembly of corrugated sheets was carried out by Luttrell,[3] El-Dakhakhni and Bryan,[4] and the author.[5] It is the author's conviction that a precise method of analysis for cylindrical shells made of corrugated sheets would open the way for another economical practical use of such material, especially because they are produced with cylindrical curvature in many countries.

In this study, the corrugated sheet assembly is treated as orthotropic material that depends on the geometrical corrugation configuration. The mathematical formulations of the theoretical model are derived, and the method of solution is given. Seismic forces are not included in the present study.

Simplified formulas and tables are prepared for use in practice to calculate the stress resultants and displacement components of the loaded shell roof.

An experimental program was undertaken in the course of the present study. The experimental results showed good agreement with those obtained theoretically.

Mathematical Formulations

The corrugated sheet assembly is treated as orthotropic material in which the mechanical properties are equal to the average properties of the corrugated sheets. For the type of corrugation used in this study (arc-and-tangent), as shown in Figure 1, the mechanical properties are:[6]

$$D_x = \left[\frac{Et}{6(1-\mu^2)}\right]\left[\frac{t}{f}\right]^2 \qquad [1\text{-a}]$$

$$D_\varphi = \left[\frac{l}{c}\right] tE \qquad [1\text{-b}]$$

$$D_{x\varphi} = p\left[\frac{c}{l}\right]\left[\frac{Et}{2(1+\mu)}\right] \qquad [1\text{-c}]$$

$$B_x = \left[\frac{c}{l}\right]\left[\frac{Et^3}{12(1+\mu^2)}\right] \qquad [1\text{-d}]$$

$$B_\varphi = 0.522\, Etf^2 \qquad [1\text{-e}]$$

$$B_{x\varphi} = \left[\frac{l}{c}\right]\left[\frac{Et^3}{12(1+\mu)}\right] \qquad [1\text{-f}]$$

in which: D_x and D_φ are the axial rigidity in the x- and φ-directions, respectively; D_x=shear rigidity in the x-φplane; B_x and B_φ are the bending rigidity in the zx- and φz-planes, respectively; $B_{x\varphi}$=torsional rigidity; t=average thickness of the sheet; c=corrugation pitch; l=developed length of corrugation per pitch; f=half depth of corrugation; E=modulus of elasticity of steel; μ=Poisson's ratio; and l=a reduction factor to account for the effect of slip at sheet-to-sheet and sheet-to-

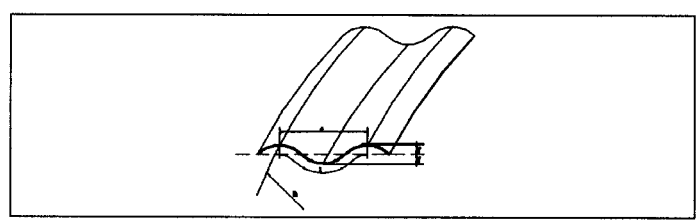

Figure 1: *Arc-and-tangent type of corrugation.*

frame connections.[1] These properties were verified experimentally.[5]

Using these notations and referring to Figure 2, the equilibrium equations may be simplified after eliminating the transverse shear to take the form:

$$N'_x + \left[\frac{N^{\circ}_{x\varphi}}{R}\right] + P_x = 0 \qquad [2\text{-a}]$$

$$RN^{\circ}_{\varphi} + R^2N'_{x\varphi} - M^{\circ}_{\varphi} - RM'_{x\varphi} + R^2p_{\varphi} = 0 \qquad [2\text{-b}]$$

$$M^{\circ\circ}_{\varphi} + RM'^{\circ}_{x\varphi} + RM'^{\circ}_{\varphi x} + R^2M''_x + RN_{\varphi} + R^2p_z = 0 \qquad [2\text{-c}]$$

$$R(N_{x\varphi} - N_{\varphi x}) + M_{x\varphi} = 0 \qquad [2\text{-d}]$$

where: $(\ )' = \frac{\partial}{\partial x}(\ )$ & $(\ )^{\circ} = \frac{\partial}{\partial \varphi}(\ )$

Using the geometric and elastic relationships of cylindrical shells[7] and substituting these into Equations 2-a, 2-b, and 2-c leads to the following governing differential equations (Equations 3-a, 3-b, and 3-c) while Equation 2-d is self-satisfied:

$$D_x u'' + \left(\frac{B_x}{R}\right)w''' + D_{x\varphi}\left[\left(\frac{1}{R^2}\right)\ddot{u} + \left(\frac{1}{R}\right)v''\right] + \left(\frac{B_{x\varphi}}{2R^2}\right)\left[\left(\frac{1}{R}\right)\ddot{u} - w''\right] + P_x = 0 \qquad [3\text{-a}]$$

$$D_{\varphi}(\ddot{v} - \dot{w}) + D_{x\varphi}\left(Ru'' + R^2v''\right) + \left(\frac{3B_{x\varphi}}{2}\right)(\dot{v}'' + \dot{w}'') + R^2p_{\varphi} = 0 \qquad [3\text{-b}]$$

$$D_{\varphi}(\ddot{v} - \dot{w}) - \left(\frac{B_{\varphi}}{R^2}\right)(\ddot{w}'' + 2\ddot{w} + w) - (R^2B_x w'''' + RB_x u''') - \left[2B_{x\varphi}\dot{w}'' + \left(3\frac{B_{x\varphi}}{2}\right)\dot{v}'' - \left(\frac{B_{x\varphi}}{2R}\right)\dot{u}''\right] + R^2p_z = 0 \qquad [3\text{-c}]$$

METHOD OF SOLUTION

The solution is carried out in three steps:

(1) A membrane solution with the surface loads acting on the shell roof.
(2) A bending solution of the unloaded shell.
(3) Superposition of the results of (1) and (2) to satisfy the boundary conditions that exist along the straight edges of the shell roof.

Membrane Solution

In the membrane solution, the shell is idealized as a membrane incapable of resisting any bending stresses. Thus omitting all terms due to bending in the equilibrium equations, the following system of equations is obtained:

$$N_x' + \left[\frac{N^{\circ}_{x\varphi}}{R}\right] p_x = 0 \qquad [4\text{-a}]$$

$$RN^{\circ}_{\varphi} + R^2N_{x\varphi} + R^2p_{\varphi} = 0 \qquad [4\text{-b}]$$

$$RN_{\varphi} + R^2p_z = 0 \qquad [4\text{-c}]$$

The following summarizes the membrane solution under different cases of loadings:

Membrane Solution Under Own Weight

The own weight, g, can be expressed in a Fourier series as:

$$g = \frac{4g}{\pi}\left[\cos\frac{\pi x}{L} - \frac{1}{3}\cos\frac{3\pi x}{L} + \frac{1}{5}\cos\frac{5\pi x}{L} \ldots\ldots\right]$$

Whenever the load is uniform in the x-direction, it is usually adequate to consider the first term of the series. Using the equilibrium equations (Equations 3-a, 3-b, and 3-c) and substituting for the load components in the x-, φ- and z-directions, the membrane solution for the stress resultants and displacement components are obtained as follows:

$$N_x = -\left(\frac{8gL^2}{R\pi^3}\right)\cos(\varphi_e - \varphi)\cos(kx) \qquad [5\text{-a}]$$

$$N_{\varphi} = -\left(\frac{4gR}{\pi}\right)\cos(\varphi_e - \varphi)\cos(kx) \qquad [5\text{-b}]$$

$$N_{x\varphi} = -\left(\frac{8gL}{\pi^2}\right)\sin(\varphi_e - \varphi)\sin(kx) \qquad [5\text{-c}]$$

$$u = \left[\frac{-8g}{Rk^3D_x}\right]\cos(\varphi_e - \varphi)\sin(kx) \qquad [5\text{-d}]$$

$$v = -\left[\frac{8g}{\pi}\right]\left[\left(\frac{1}{k^3D_{x\varphi}}\right) + \left(\frac{1}{R^2k^4Dx}\right)\right]\sin(\varphi_e - \varphi)\cos(kx) \qquad [5\text{-e}]$$

$$w = \left[\frac{8g}{\pi}\right]\left[\left(\frac{1}{k^3D_{x\varphi}}\right) + \left(\frac{1}{R^2k^4Dx}\right)\right]\cos(\varphi_e - \varphi)\cos(kx) \qquad [5\text{-f}]$$

in which $k = \frac{\pi}{L}$

Membrane solution under snow load p

The snow load can be expressed in a Fourier series as follows:

$$p = \left[\frac{4p\cos(\varphi_e - \varphi)}{\pi}\right]\left[\cos\frac{\pi x}{L} - \frac{1}{3}\cos\frac{3\pi x}{L} + \ldots\ldots\right]$$

As in the case of the own weight, g, the load is uniform in the x-direction and the first term in the series is usually sufficient. Substituting for the three load components in the x-, φ- and z-directions, the corresponding stress resultants and displacement components are obtained as follows:

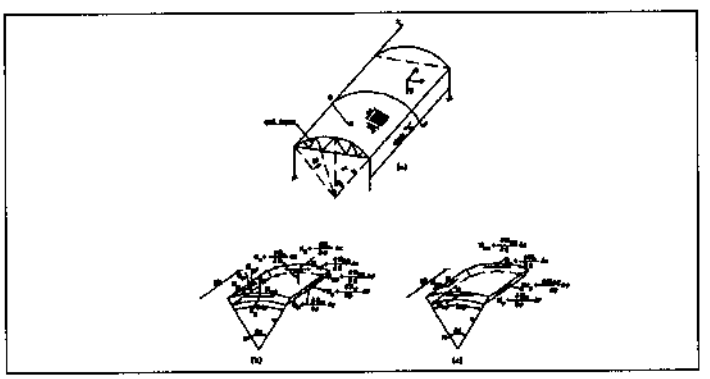

Figure 2: (a): Coordinate System (b): Stress Results N_x, N_{φ}, $N_{x\varphi}$ (c): Moments M_x, M_{φ}, $M_{x\varphi}$

$$N_\varphi = -\left(\frac{4pL}{\pi}\right)(\cos(\varphi_e - \varphi))^2 \cos(kx) \quad [6\text{-a}]$$

$$N_x = -\left(\frac{12p}{R\pi k^2}\right)\cos 2(\varphi_e - \varphi)\cos(kx) \quad [6\text{-b}]$$

$$N_{x\varphi} = \left(\frac{6pL}{\pi^2}\right)\sin 2(\varphi_e - \varphi)\sin(kx) \quad [6\text{-c}]$$

$$u = -\left[\frac{12p}{Rk\pi^3 D_x}\right]\cos 2(\varphi_e - \varphi)\sin(kx) \quad [6\text{-d}]$$

$$v = -\left[\frac{6p}{\pi}\right]\left[\left(\frac{1}{k^2 D_{x\varphi}}\right) + \left(\frac{4}{R^2 k^4 Dx}\right)\right]\sin 2(\varphi_e - \varphi)\cos(kx) \quad [6\text{-e}]$$

$$w = \left[\frac{12p}{\pi}\right]\left[\left(\frac{1}{k^2 D_{x\varphi}}\right) + \left(\frac{4}{R^2 k^4 D_x}\right)\right]\cos 2(\varphi e - \varphi)\cos(kx) \quad [6\text{-f}]$$

If isotropic properties are considered, the previously given values for stress resultants and displacement components yield the well-known values of the membrane solution for isotropic shells.

Membrane solution under wind loading

Many factors affect wind load on shell roofs. The load may take any asymmetrical shape, depending on the geometrical dimensions of the shell and the direction of the wind. The effects of asymmetrical loading may be divided into two cases—one symmetrical and the other asymmetrical. It is possible to obtain the solution under any case of loading, using the principle of superposition.

Bending Solution

The loading is considered in the membrane solution, then p_x, p_φ and p_z are replaced by zero in Equations 3-a, 3-b, and 3-c. Taking into account the coordinate system shown in Figure 2, the bending solution can be expressed in a Levy-type solution as follows:

$$w = A^* e^{m\varphi}\cos\left(\frac{\lambda x}{R}\right) \quad [7\text{-a}]$$

$$u = B^* e^{m\varphi}\sin\left(\frac{\lambda x}{R}\right) \quad [7\text{-b}]$$

$$v = C^* e^{m\varphi}\cos\left(\frac{\lambda x}{R}\right) \quad [7\text{-c}]$$

where $\lambda = \dfrac{\pi R}{L}$

Substituting Equations 7-a, 7-b, and 7-c into Equations 3-a, 3-b, and 3-c after replacing the load components by zero as mentioned before, the resulting homogeneous system of equations can be written in a matrix form as:

$$\begin{bmatrix} -D_x\lambda^2 + D_{x\varphi}m^2 + K_{x\varphi}m^2 & -D_{x\varphi}m\lambda & -K_x\lambda^3 - K_{x\varphi}m^2 \\ D_{x\varphi}m\lambda & D_\varphi m^2 - D_{x\varphi}\lambda^2 - 3K_{x\varphi}\lambda^2 & D_\varphi m + 3K_{x\varphi}m\lambda^2 \\ K_x\lambda^3 + k_{x\varphi}m^2\lambda & D_\varphi m + 3K_{x\varphi}m\lambda^2 + K_{x\varphi}m\lambda & D_\varphi + K_\varphi m^4 + 2K_\varphi m^2 + K_\varphi + K_x\lambda^4 - 4K_{x\varphi}m^2\lambda^2 \end{bmatrix}\begin{bmatrix} A^* \\ B^* \\ C^* \end{bmatrix} = 0$$

A nontrivial solution of this system of equations can be obtained only if the determinant of the left-hand matrix is equal to zero. The final form of this equation takes the following form:

$$m^8 + m^6\left[2 - \lambda^2\left(\frac{D_x}{D_{x\varphi}} + \frac{2B_{x\varphi}}{B_\varphi}\right)\right] + m^4\left[\lambda^4\left(\frac{D_x}{D_\varphi} + \frac{2D_x 2B_{x\varphi}}{D_{x\varphi}B_\varphi} + \frac{B_x}{B_\varphi}\right) - \lambda^2\left(\frac{2D_x}{D_{x\varphi}} + \frac{4D_{x\varphi}}{B}\right) + 1\right]$$
$$m^2\left[-\lambda^6\left(\frac{D_x B_x}{D_{x\varphi}B_\varphi} + \frac{2D_x B_{x\varphi}}{D_\varphi B_\varphi}\right) + \lambda^4\left(\frac{2D_x}{D_\varphi} - \frac{2B_x}{B_\varphi} + \frac{3D_x B_{x\varphi}}{D_{x\varphi}B_\varphi}\right) - \lambda^2\left(\frac{2B_{x\varphi}}{B_\varphi} + \frac{D_x}{D_{x\varphi}}\right)\right]$$
$$+\left[\lambda^8\left(\frac{D_x B_x}{D_\varphi B_\varphi}\right) + \lambda^4\left(\frac{R^2 D_x}{B_\varphi} + \frac{3D_x B_{x\varphi}}{2D_{x\varphi}B_\varphi}\right) + \frac{D_x}{D_\varphi}\right] = 0 \quad [8]$$

Equation 8 is the characteristic equation of orthotropic cylindrical shells. If isotropic properties are considered, it yields the well-known Flügge[7] (Dischinger) characteristic equation for isotropic shells.

The roots of this equation can be written as $m = \pm\alpha_1 \pm i\beta_1$, $m = \alpha_2 \pm i\beta_2$, where $i = \sqrt{-1}$.

Substituting for these roots back into Equation 7-a, the displacement, w, can be written as:

$$w = [e^{\alpha_1\varphi}(A\cos(\beta_1\varphi) + B\sin(\beta_1\varphi)) + e^{-\alpha_1\varphi}(C\cos(\beta_1\varphi) + D\sin(\beta_1\varphi))$$
$$+e^{\alpha_2\varphi}(E\cos(\beta_2\varphi) + F\sin(\beta_2\varphi)) + e^{-\alpha_2\varphi}(G\cos(\beta_2\varphi)) + H\sin(\beta_2\varphi))]\cos\left(\frac{\lambda x}{R}\right) \quad [9]$$

where A, B, C...H are arbitrary real constants to be determined by satisfying the boundary conditions along the straight edges of the shell roof. (See Figure 3.)

THEORETICAL RESULTS

A computer program exists for all possible boundary conditions that may exist along the straight edges of the shell. The following simplified formulas may be used to evaluate the stress resultants at any point on the shell surface.

$$N_x = \breve{N}_x\, p\cos\left(\frac{\pi x}{L}\right) \quad [10\text{-a}]$$

$$N_\varphi = \breve{N}_\varphi\, p\cos\left(\frac{\pi x}{L}\right) \quad [10\text{-b}]$$

$$N_{x\varphi} = \breve{N}_{x\varphi}\, p\sin\left(\frac{\pi x}{L}\right) \quad [10\text{-c}]$$

$$M_\varphi = \breve{M}_\varphi\, p\cos\left(\frac{\pi x}{L}\right) \quad [10\text{-d}]$$

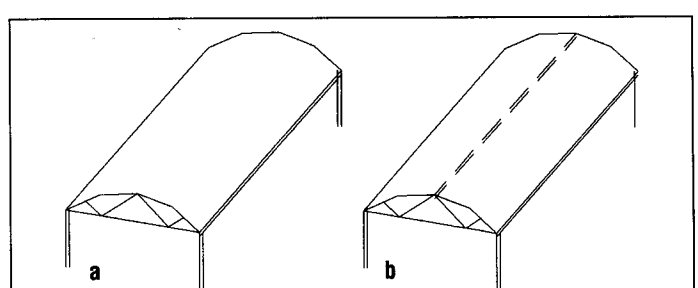

Figure 3. (a) case I (simple span), longitudinal stiffeners along valleys only and (b) case II (simple span), longitudinal stiffeners along valleys and crown.

where p is the intensity of snow load and the bar-indicated symbols are values obtained directly from the computer output.

If other intensity of loading or case of boundary conditions are required, the membrane solution and the case of boundary conditions are simply chosen in the program input.

Appendix I is an output of results for a shell roof of span L=6.0 m (10 feet) and radius=3.0 m (10 feet) where the angle $\varphi e=80°$. The shell is made up of corrugated sheets with gauge 22 and uses longitudinal stiffeners of cold-rolled angles (63.5 by 63.5 by 6.35 mm [2.5 by 2.5 by 0.25 inches]) along the straight edges. The intensity of snow load is considered 720 N/m^2 (15 psf).

EXPERIMENTAL VERIFICATION

An experimental program was undertaken with full-scale shell roofs using two cases of boundary conditions: The first was a shell roof with longitudinal stiffeners in the valleys only, and the other used a longitudinal stiffener in the crown in addition to the ones along the valleys, as shown in Figure 3. Snow load effect was simulated using high strength wires through the used bolts for connecting the sheets, as shown in Figure 4-c. No uplift was experimentally verified.

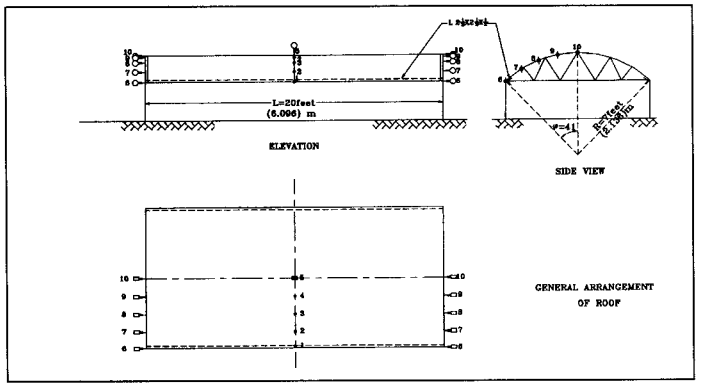

Figure 4-a.

All parameters and geometry of the tested shells are indicated in the figures.

Displacement components u, v, and w were measured in each experiment under different increments of loading, and the comparison shown in Figures 5-a, 5-b, and 5-c proves good agreement between the theoretical values and the corresponding experimentally measured values for the deflection of the crown point at mid-span, for N_x-distribution along the circumference at mid-span, and the u-displacements at support, respectively.

SIMPLIFIED FORMULAS

The final equations giving values for all stress resultants and displacement components at any point on the shell surface are very lengthy. A computer program has been written to solve the two boundary conditions mentioned earlier. Equations 10-a through 10-d can easily be used with the help of tables that are given in Appendix I. Appendix II, shows a demonstration of using these tables together with the simplified formulas.

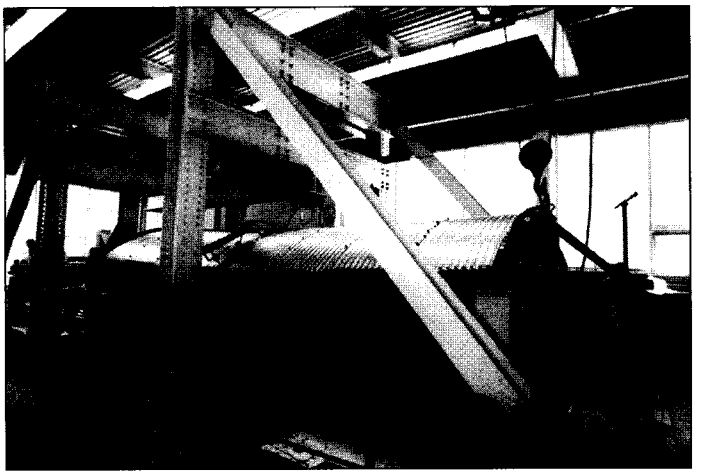

Figure 4-b. A picture of the shell model.

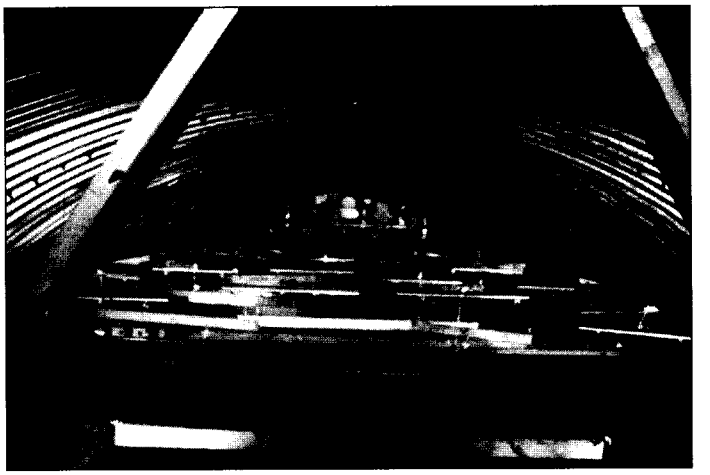

Figure 4-c. A picture of the loading system.

REFERENCES

1. Nilson, A. H. "Shear Diaphragms of Light Gage Steel," *Journal of the Structural Division*, ASCE, Vol. 86, ST11, November 1960.
2. Nilson, A. H. "Folded Plate Structures of Light Gage Steel," *ASCE Transactions Paper*, No. 3514, Vol. 128, Part (II), 1963, 848-880.
3. Luttrell, L. D. "Structural Performance of Light Gage Steel Diaphragms," *Report 319*, Department of Structural Engineering, Cornell University, August 1965.
4. El-Dakhakhni, M. W. and E. R. Bryan. "Shear of Thin Plates with Flexible Edge Members," *Proceedings of ASCE*, Vol. 90, No. ST4, August 1964.
5. El-Atrouzy, M. N. "Structural Properties of Corrugated Sheets Used in Cylindrical Shells," M.Sc. Thesis, University of Windsor, Ontario, Canada, 1969.
6. El-Atrouzy, M. N. and G. Abdel-Sayed. *Cylindrical Shells Made of Corrugated Sheets*, International Association of Bridge and Structural Engineering, 1972.
7. Flügge, W. *Stresses in Shells*, Springer-Verlag, Berlin/Gottingen/Heidelberg, 1962.

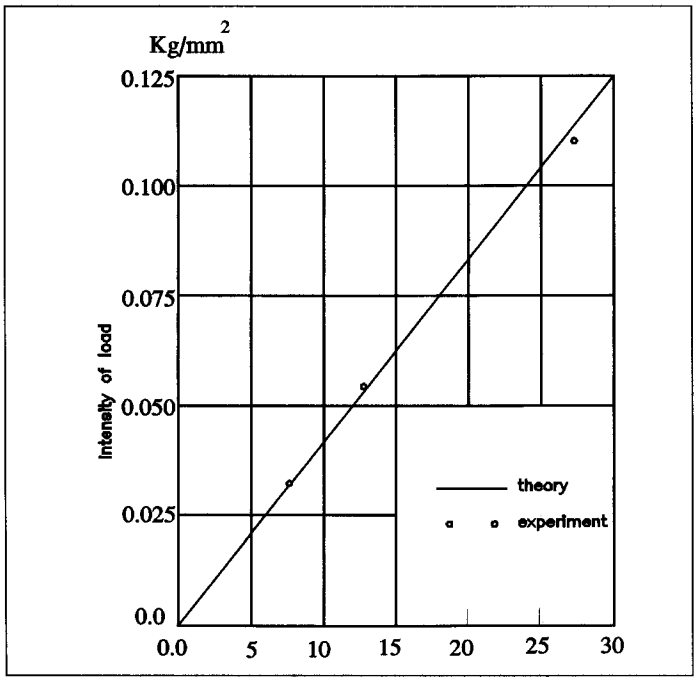

Figure 5-a. Comparison between theoretical and experimental load-deflection curves of crown point at mid-span (Experiment No. 1).

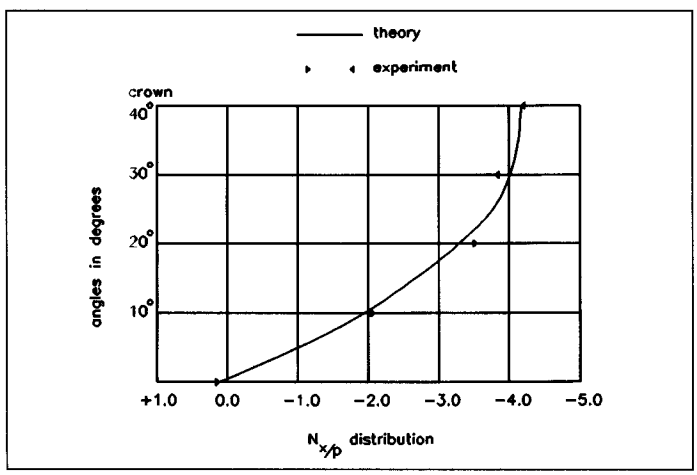

Figure 5-b. Comparison between theoretical and experimental values of U-displacement at support (Experiment No. 2).

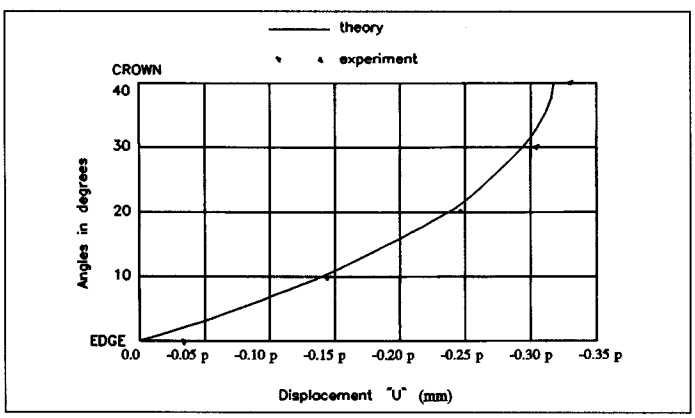

Figure 5-c. Comparison between theoretical and experimental values of U-displacement at support (Experiment No. 2).

Appendix 1

STRESS RESULTANT COEFFICIENTS USING LONGITUDINAL STIFFENERS IN VALLEYS ONLY

Boundary Conditions: Case I, Half Central Angle: ϕ_e=80°, GA 22

Radius m	Span m	ϕ/ϕ_e	N_x	N_φ	$N_{x\varphi}$	M_φ
10	15	Valley	0.0311	0.0000	0.4722	0.0000
		¼	0.2737	0.2777	0.6335	-0.0140
		½	-0.0760	-0.6137	0.7274	0.1139
		¾	-0.5428	-0.9254	0.4946	0.1979
		Crown	-0.7461	-1.0537	0.0000	0.2084
10	20	Valley	0.0311	0.0000	0.6565	0.0000
		¼	0.4355	-0.2864	0.8471	0.0148
		½	-0.1539	-0.6127	0.9416	0.2803
		¾	-0.9443	-0.9182	0.6424	0.5458
		Crown	-1.2901	-1.0414	0.0000	0.6395
10	25	Valley	0.0311	0.0000	0.8645	0.0000
		¼	0.5658	-0.2990	1.0655	0.0553
		½	-0.2918	-0.6228	1.1562	0.5197
		¾	-1.4279	-0.9076	0.7696	1.0552
		Crown	-1.9247	-1.0228	0.0000	1.2748
10	30	Valley	0.0311	0.0000	1.0908	0.0000
		¼	0.6431	-0.3121	1.2874	0.0971
		½	-0.4999	-0.6288	1.3458	0.7683
		¾	-1.9848	-0.8966	0.8812	1.5860
		Crown	-2.6324	-1.0032	0.0000	1.9375
10	35	Valley	0.0311	0.0000	1.3232	0.0000
		¼	0.6841	-0.3228	1.5106	0.1314
		½	-0.7701	-0.6338	1.5303	0.9720
		¾	-2.6219	-0.8875	0.9874	2.0214
		Crown	-3.4269	-0.9872	0.0000	2.4813
15	30	Valley	0.0311	0.0000	0.9604	0.0000
		¼	0.7129	-0.4196	1.2651	0.0110
		½	-0.2022	-0.9209	1.4490	0.3527
		¾	-1.4414	-1.3858	0.9857	0.6256
		Crown	-1.9831	-1.5773	0.0000	0.6844

Appendix 1

STRESS RESULTANT COEFFICIENTS USING LONGITUDINAL STIFFENERS IN VALLEYS AS WELL AS IN CROWN

Boundary Conditions: Case II, Half Central Angle: ϕ_e=80°, GA 22

Radius m	Span m	ϕ/ϕ_e	N_x	N_φ	$N_{x\varphi}$	M_φ
10	15	Valley	0.0311	0.0000	0.5263	0.0000
		¼	0.1076	-0.2904	0.5942	0.0603
		½	0.0181	-0.5693	0.6430	0.3491
		¾	-0.0353	-0.8814	0.6313	0.0097
		Crown	-0.0311	-1.2719	0.6062	-0.7211
10	20	Valley	0.0311	0.0000	0.7041	0.0000
		¼	0.1791	-0.2861	0.7759	0.0575
		½	1.1023	-0.5580	0.8587	0.2772
		¾	-0.0002	-0.8831	0.8842	-0.2613
		Crown	-0.0311	-1.3037	0.8723	-1.1447
10	25	Valley	0.0311	0.0000	0.8553	0.0000
		¼	0.3376	-0.2760	0.9543	0.0312
		½	0.2497	-0.5490	1.0927	0.0902
		¾	0.0526	-0.8897	1.1579	-0.7319
		Crown	-0.0311	-1.3369	1.1564	-1.7898
10	30	Valley	0.0311	0.0000	0.9811	0.0000
		¼	0.6180	-0.2628	1.1267	0.0065
		½	0.4925	-0.5384	1.3447	-0.1586
		¾	0.1352	-0.8988	1.4589	-1.3245
		Crown	-0.0311	-1.3740	1.4681	-2.5828
10	35	Valley	0.0311	0.0000	1.0900	0.0000
		¼	1.0278	-0.2495	1.2946	-0.0453
		½	0.8392	-0.5285	1.6087	-0.4085
		¾	0.2510	-0.9081	1.7793	-1.9111
		Crown	-0.0311	-1.4094	1.7997	-3.3630
15	30	Valley	0.0311	0.0000	1.0675	0.0000
		¼	0.2597	-0.4356	1.1670	0.1505
		½	0.0938	-0.8469	1.2795	0.8006
		¾	-0.0291	-1.3202	1.2896	-0.0938
		Crown	-0.0311	-1.9297	1.2712	-1.8760

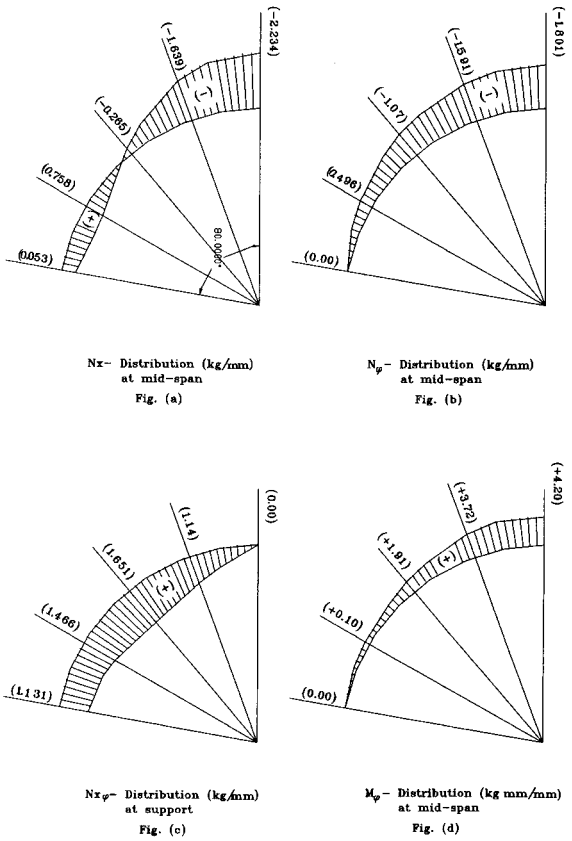

Nx- Distribution (kg/mm) at mid-span
Fig. (a)

N_φ- Distribution (kg/mm) at mid-span
Fig. (b)

$N_{x\varphi}$- Distribution (kg/mm) at support
Fig. (c)

M_φ- Distribution (kg mm/mm) at mid-span
Fig. (d)

Figure for Appendix II

Appendix 2

The analysis of a simply supported cylindrical shell roof by the use of tables will be illustrated in this example:
Design a shell roof made of corrugated sheets with longitudinal stiffeners at the valleys. The shell has the following parameters:
Span=6.10 m (20 feet)
Radius=3.05 m (10 feet)
Half the central angle φ_e=80°
Maximum intensity of snowload=73.5 kg/m² (15 psf)

Solution:
From the table in Appendix I, the roof with the given dimensions can be built with gauge 22 and can carry a maximum intensity of 97.6 kg/m² (20 psf) snow load. From Table I, the stress resultants can be calculated from the simplified formulae (i.e., Forumlae 10-a through 10-d). Figures A, B, C, and D show the distribution of the stress resultants. The required area of longitudinal stiffener = (15xL/πöx)* 0.6565=76.1 mm² (0.118 in²).